Approximate Viscous Shock-Layer Method for Hypersonic Flow over Blunt-Nosed Bodies

A. C. Grantz* and F. R. DeJarnette†
North Carolina State University, Raleigh, North Carolina 27695
and
R. A. Thompson‡
NASA Langley Research Center, Hampton, Virginia 23665

An approximate axisymmetric method is presented that can calculate the surface and flowfield properties accurately for the fully viscous hypersonic flow over blunt-nosed bodies. Using the second-order pressure equation of Maslen and incorporating viscous terms into the streamwise momentum and energy equations, a simple method is obtained which can calculate both the subsonic and supersonic regions of the shock layer and does not require a starting solution for the shock shape. The turbulence model of Cebeci-Smith and the equilibrium air tables of Hansen are incorporated into the method. The method is faster than the parabolized Navier-Stokes or viscous shock-layer solvers it might replace in a preliminary design environment. Hyperboloid and sphere cone configurations at 0-deg angle of attack and with half-angles up to 45 deg have been successfully run to convergence. Surface heat-transfer and pressure predictions from the present method compare very well with the more accurate viscous shock-layer method, flight and wind-tunnel data. Distributions of flowfield properties across the shock layer also compare very well between the two methods. Because the present viscous method does not require a starting solution, it could be used to provide more accurate shock shapes for higher-order methods which currently use inviscid starting solutions.

Nomenclature

C_p = specific heat at constant pressure, divided by $u_\infty^2/T_\infty/2$
F = ratio of local-to-shock tangential velocity, u/u_s
H = total enthalpy, $H = h + u^2/2 + v^2/2$, divided by H_∞
h = enthalpy, divided by $u_\infty^2/2$
h_1, h_3 = curvilinear coordinate metrics, divided by R_n
k = thermal conductivity, Btu/ft s °R
M = Mach number
n = inward normal distance from the shock, divided by R_n
Pr = Prandtl number, $\mu C_p/k$
p = pressure, divided by $\rho_\infty u_\infty^2$
$\dot{q}$ = heat-transfer rate, Btu/ft^{2}s
R = radius of curvature, divided by R_n
Re = Reynolds number, $\rho_\infty u_\infty R_n/\mu_\infty$
r = radius, divided by R_n
s = distance along the shock, divided by R_n
T = temperature, divided by T_∞
T_{ref} = $T_{\text{ref}} = u_\infty^2/Cp_\infty$
u = tangential velocity, divided by u_∞
v = normal velocity, divided by u_∞
$\bar{x}, \bar{y}$ = Cartesian coordinate system, divided by R_n
α, β = shock stretching factors
Γ = body or shock angle referenced to freestream velocity vector
γ = ratio of specific heats
η = Ψ/Ψ_s
ϵ = $\epsilon = [\rho_\infty u_\infty R_n/\mu(T_{\text{ref}})]^{-1/2}$
κ = curvature, $1/R$
μ = dynamic viscosity, divided by μ_∞
Ψ = stream function, divided by $\rho_\infty u_\infty R_n^2$
ρ = density, divided by ρ_∞

Subscripts
b = body
n = nose
o = stagnation point
s = shock
w = wall
∞ = freestream

Superscript
$\bar{F}$ = value of F from previous linearization step

Introduction

AT the relatively low Reynolds numbers encountered by hypersonic vehicles at high altitude, the viscous layer is a significant fraction of the shock layer. Accurate predictions of the flowfield properties typically require solutions to the Navier-Stokes, the parabolized Navier-Stokes,[1,2] or the viscous shock-layer[3,4] equations. Unfortunately, existing methods for solving these equations require more computational effort than can be tolerated for preliminary design studies. An approximate method that can provide quick and economical engineering estimates is required.

For larger Reynolds numbers, the shock layer is characterized by a boundary layer that is very thin in comparison to the outer inviscid layer. Using an inviscid method, the flow properties are calculated along the body surface. A boundary-layer solver then can be used to calculate the desired heating and skin-friction distribution.[5] Unfortunately, the highly curved shock produced by a blunt-nosed body introduces strong entropy gradients into the inviscid flow, which compli-

Presented as Paper 89-1695 at the AIAA 24th Thermophysics Conference, Buffalo, NY, June 12-14, 1989; received June 26, 1989; revision received March 8, 1990.

*Research Assistant; currently Aerospace Engineer, NAA, Rockwell International. Member AIAA.
†Professor, Mechanical and Aerospace Engineering. Associate Fellow AIAA.
‡Aerospace Technologist, Aerothermodynamics Branch. Member AIAA.

cates determining the boundary-layer edge conditions. Mass balancing[6,7] and interpolation into the inviscid layer[8,9] are two techniques frequently used to account for variable entropy layers.[10] Several investigators have used variations of the method of Maslen[11,12] coupled with boundary-layer methods to solve high Reynolds number flows. Zoby and Simmonds[10] extended the method of Ref. 13 to calculate heat-transfer rates in perfect gas and equilibrium air flows at both constant and variable entropy conditions. Grose[14] used Maslen's original inverse method and a nonequilibrium chemistry model to compute the flowfields over hyperboloids and blunt bodies of revolution during Jovian and Venusian atmospheric-entry freestream conditions. Most of these methods neglect the effects of the boundary layers on the inviscid layer and the shock surface shape. Davis[15] described a method for coupling the interaction of the two layers through the boundary-layer displacement thickness. However, for low Reynolds number flows, where the viscous layer is a significant fraction of the shock layer and has a strong effect on the shock shape, simply coupling a boundary-layer method to an inviscid solution would yield unsatisfactory results.

The current research deviates from previous work with the method of Maslen in that the viscous layer is solved as part of the total flowfield solution. By incorporating boundary-layer-like viscous terms into the streamwise momentum and energy equations, and utilizing Maslen's second-order approximate integral to the normal momentum equation, a parabolic equation set is obtained. The viscous terms are retained across the entire shock layer to avoid the problems associated with matching boundary-layer edge conditions. A relatively simple method is developed which is valid in both the subsonic and supersonic regions of the shock layer and is self-starting. Phenomenological models, which account for transition, turbulence, and equilibrium air chemistry are easily incorporated because of the method's simplicity. The present method serves as the foundation for a three-dimensional, viscous-flow method currently under development. Prior to extending the method to treat more complex flowfields, it is essential that the approximations made be validated for the simpler axisymmetric case. The purpose of this paper is to demonstrate the applicability of the axisymmetric method by comparing the heating and pressure predictions with flight and wind-tunnel data as well as with the more detailed viscous shock-layer method.

Viscous Shock-Layer Equations

The viscous shock-layer (VSL) equations are a subset of the compressible Navier-Stokes equations in which parabolic approximations are made in both the streamwise and crossflow directions as follows. The conservation equations are nondimensionalized in both the inviscid outer region and the inner viscous region (boundary layer) with variables that are of order one. Terms in each of the two resulting sets of equations are retained up to second-order in the parameter ϵ. By combining the two equations sets, a single set of equations that is uniformly accurate to second-order in both the inner and outer regions of the shock layer is obtained. To serve as a point of reference in the discussions to follow, the axisymmetric form of the VSL equations for a body-oriented coordinate system as written by Anderson and Moss[16] are presented below:

Continuity:

$$\frac{\partial}{\partial s}\left(\rho u h_3\right) + \frac{\partial}{\partial n}\left(\rho v h_1 h_3\right) = 0 \tag{1}$$

s-momentum:

$$\rho\left(\frac{u}{h_1}\frac{\partial u}{\partial s} + v\frac{\partial u}{\partial n} + \frac{uv}{h_1}\frac{\partial h_1}{\partial n}\right) + \frac{1}{h_1}\frac{\partial p}{\partial s} = \epsilon^2\left\{\frac{\partial}{\partial n}\left[\mu\left(\frac{\partial u}{\partial n} - \frac{u}{h_1}\frac{\partial h_1}{\partial n}\right)\right] + \mu\left(\frac{2}{h_1}\frac{\partial h_1}{\partial n} + \frac{1}{h_3}\frac{\partial h_3}{\partial n}\right)\left(\frac{\partial u}{\partial n} - \frac{u}{h_1}\frac{\partial h_1}{\partial n}\right)\right\} \tag{2}$$

n-momentum:

$$\rho\left(\frac{u}{h_1}\frac{\partial v}{\partial s} + v\frac{\partial v}{\partial n} - \frac{u^2}{h_1}\frac{\partial h_1}{\partial n}\right) + \frac{\partial p}{\partial n} = 0 \tag{3}$$

Energy:

$$\rho\left(\frac{u}{h_1}\frac{\partial H}{\partial_s} + v\frac{\partial H}{\partial n} + \frac{\rho u^2 v}{h_1}\frac{\partial h_1}{\partial n}\right) - v\frac{\partial p}{\partial n} = \epsilon^2\left\{\frac{\partial}{\partial n}\left[\frac{\mu}{Pr}\frac{\partial H}{\partial n} + \left(\mu - \frac{\mu}{Pr}\right)\frac{1}{2}\frac{\partial u^2}{\partial n} - \frac{\mu u^2}{h_1}\frac{\partial h_1}{\partial n}\right] + \left(\frac{1}{h_1}\frac{\partial h_1}{\partial n} + \frac{1}{h_3}\frac{\partial h_3}{\partial n}\right) \times \left[\frac{\mu}{Pr}\frac{\partial H}{\partial n} + \left(\mu - \frac{\mu}{Pr}\right)\frac{1}{2}\frac{\partial u^2}{\partial n} - \frac{\mu u^2}{h_1}\frac{\partial h_1}{\partial n}\right]\right\} \tag{4}$$

For these equations only, s and n refer to body normal and tangential directions, respectively, where $h_1 = 1 + n\kappa_b$, $h_3 = r$, and

$$H = h + \frac{u^2}{2}, \qquad \mu = \frac{\mu}{\mu(T_{\text{ref}})} \tag{5}$$

Although the VSL equations have been parabolized in the streamwise direction, the derivatives dn_s/ds_b and $\partial v/\partial s$ introduce an elliptic effect into the equations. Anderson and Moss[16] neglect these terms during the first global iteration in which a thin stock layer is assumed. During the second global iteration, the derivatives are retained and calculated using information from the previous iteration. Murray and Lewis[4,17] obtain dn_s/ds_b from an inviscid solution, and the values of $\partial v/\partial s$ are calculated from a backward difference. This procedure reduces the need for several global iterations provided the starting shock shape is suitably accurate. During the analysis of the approximate method proposed in this paper, comparisons will be made to the VSL method of Ref. 17.

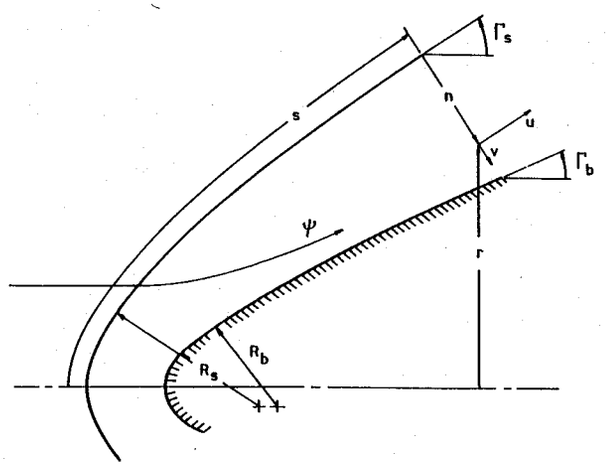

Fig. 1 Shock-oriented coordinate system for axisymmetric flow.

Approximate Method

Because the original inviscid Maslen method was an inverse technique, it was appropriate to employ a shock-oriented coordinate system as illustrated in Fig. 1. A von Mises transformation was made to introduce the independent variables s and

Ψ into the momentum equations. The momentum equation normal to the shock was given by

$$\left(1-n\kappa_s\right)\frac{\partial p}{\partial \Psi}=\frac{u}{Rr}+\frac{1}{r}\left(\frac{\partial v}{\partial s}\right) \tag{6}$$

Continuity was satisfied by the definition of the stream function:

$$\frac{\partial \Psi}{\partial n}=-\rho u r, \qquad \frac{\partial \Psi}{\partial s}=\rho v r\left(1-n\kappa_s\right) \tag{7}$$

Neglecting v, the energy equation was

$$h_{so}=h(s,\Psi)+u^2(s,\Psi) \tag{8}$$

The condition of constant entropy along a streamline was also used:

$$S=S(\Psi) \tag{9}$$

One important feature of Maslen's methods was the approximate integrals of the normal momentum equation he developed. In his 1964 paper, Maslen[11] neglected the second term of the normal momentum equation given above by assuming that it was negligible in comparison to the first term. He also noticed that a fortuitous partial cancellation of errors occurred if he evaluated the first term on the right-hand side of the equation at the shock instead of using the local values within the shock layer. The equation

$$\frac{\partial p}{\partial \Psi}\approx\frac{u_s}{R_s r_s} \tag{10}$$

was then easily integrated:

$$p(s,\Psi)=p_s(s)+\frac{u_s(s)}{r_s(s)R_s(s)}\left[\Psi-\Psi_s(s)\right] \tag{11}$$

Unfortunately, this first-order approximate integral to the normal momentum equation did not accurately predict the pressure in the stagnation region for blunt-nosed bodies.[13] Maslen later retained the second term by assuming that the normal velocity gradient within the shock layer was proportional to its value at the shock[12]:

$$\frac{\partial v}{\partial s}\approx\left(\frac{\partial v}{\partial s}\right)_s\eta \tag{12}$$

For smooth shock surfaces and hypersonic speeds, Maslen also noted that at the shock

$$\frac{\partial v}{\partial s}-\frac{v_s}{p_s}\frac{\partial \rho}{\partial s}\approx 0 \tag{13}$$

These assumptions led to Maslen's second-order approximate integral to the normal momentum equation

$$p\left(s,\Psi\right)=p_s+\frac{u_s}{R_s r_s}\left(\Psi-\Psi_s\right)$$

$$-\frac{v_s\tan\Gamma_s}{r_s}\left(\kappa_s+\frac{\cos\Gamma_s}{r_s}\right)\frac{\left(\Psi^2-\Psi_s^2\right)}{2\Psi_s} \tag{14}$$

For the analysis here, add boundary-layer viscous terms to the streamwise momentum and energy equations. The momentum equation along a streamline becomes

$$\frac{\rho}{2}\left(\frac{\mathrm{D}u^2}{\mathrm{D}s}+\frac{\mathrm{D}v^2}{\mathrm{D}s}\right)+\frac{\mathrm{D}p}{\mathrm{D}s}=\frac{1-\kappa_s n}{Re}\frac{\partial}{\partial n}\left[\mu\frac{\partial u}{\partial n}\right] \tag{15}$$

To be consistent, however, the viscous term must be transformed into the streamline coordinate system. Applying the operator

$$\frac{\partial}{\partial n}=\frac{\partial \Psi}{\partial n}\frac{\partial}{\partial \Psi}=-\rho u r\frac{\partial}{\partial \Psi} \tag{16}$$

to the viscous term yields

$$\frac{\rho}{2}\left(\frac{\mathrm{D}u^2}{\mathrm{D}s}+\frac{\mathrm{D}v^2}{\mathrm{D}s}\right)=-\frac{\mathrm{D}p}{\mathrm{D}s}$$

$$+\frac{1-\kappa_s n}{Re}\left(-\rho u r\right)\frac{\partial}{\partial \Psi}\left[\left(-\rho u r\right)\mu\frac{\partial u}{\partial \Psi}\right] \tag{17}$$

Similarly, by adding boundary-layer-like viscous terms to the energy equation

$$\rho u\frac{\mathrm{D}H}{\mathrm{D}s}=\frac{1-n\kappa_s}{Re}\left\{\frac{\partial}{\partial n}\left[\frac{\mu}{Pr}\frac{\partial H}{\partial n}+\left(\mu-\frac{\mu}{Pr}\right)\frac{1}{2}\frac{u_\infty^2}{H_\infty}\frac{\partial u^2}{\partial n}\right]\right\}$$

and transforming the right-hand side into streamline coordinates, there results

$$\rho u\frac{\mathrm{D}H}{\mathrm{D}s}=\frac{1-n\kappa_s}{Re}\left\{(\rho u r)\frac{\partial}{\partial \Psi}\left[(\rho u r)\frac{\mu}{Pr}\frac{\partial H}{\partial \Psi}\right.\right.$$

$$\left.\left.+(\rho u r)\left(\mu-\frac{\mu}{Pr}\right)\frac{1}{2}\frac{u_\infty^2}{H_\infty}\frac{\partial u^2}{\partial \Psi}\right]\right\}$$

Unfortunately, derivatives with respect to the stream function Ψ are not well defined in the stagnation region of blunt-nosed bodies. In order to make the governing equations applicable throughout the entire shock layer, the variable $\eta=\Psi/\Psi_s$ is used where η varies from zero at the body to one at the shock. The transformation operators from (s,Ψ) to (s,η) are given below:

$$\frac{\mathrm{D}}{\mathrm{D}s}=\frac{\partial}{\partial s}\bigg|_\eta+\frac{\mathrm{D}\eta}{\mathrm{D}s}\frac{\partial}{\partial \eta}\bigg|_s=\frac{\partial}{\partial s}\bigg|_\eta-\frac{\eta r_s\sin\Gamma_s}{\Psi_s}\frac{\partial}{\partial \eta} \tag{18}$$

$$\frac{\partial}{\partial \Psi}=\left(\frac{\partial \eta}{\partial \Psi}\right)_s\frac{\partial}{\partial \eta}=\frac{1}{\Psi_s}\frac{\partial}{\partial \eta} \tag{19}$$

Applying these transformations to the streamwise momentum equation and then simplifying yields the following results:

$$r_s u_s\frac{\partial F^2}{\partial r_s^2}+\kappa_s F^2-\left[\eta\frac{u_s}{r_s}+\frac{u_s^2}{r_s^2}\frac{\mu}{Re\sin\Gamma_s}\right]\frac{\partial F^2}{\partial \eta}$$

$$-\frac{2}{Re\sin\Gamma_s}\frac{u_s^2}{r_s^2}\left(\frac{r}{r_s}\right)^2F\frac{\partial}{\partial \eta}\left[\rho\mu\frac{\partial F^2}{\partial \eta}\right]$$

$$=-\frac{r_s}{u_s}\frac{\partial v^2}{\partial r_s^2}-\frac{1}{\rho u_s\sin\Gamma_s}\frac{\partial p}{\partial s}$$

$$+\frac{2\eta}{r_s u_s}\left[\frac{1}{\rho}\frac{\partial p}{\partial \eta}+\frac{1}{2}\frac{\partial v^2}{\partial \eta}-\frac{\mathrm{d}H^\circ(\eta)}{\mathrm{d}\eta}\right] \tag{20}$$

where

$$F^2=\left(\frac{u}{u_s}\right)^2 \tag{21}$$

The quantity $\mathrm{d}H^\circ(\eta)/\mathrm{d}\eta$ is added to force the terms within the square bracket to sum to zero so that the equation will be consistent in the limit as $s\to 0$. The equation is cast in terms of the variable F^2 because the square of the tangential velocity component, u^2, appears more often than u. This substitutaion of dependent variables will facilitate the quasilinearization process necessary to solve the governing equations. Addition-

ally, choosing F^2 for the dependent variable removes a singularity at the wall when calculating skin friction. The partial derivative $\partial/\partial s$ was replaced by $2r_s \sin\Gamma_s \partial/\partial r_s^2$ since r_s^2 is a more readily available independent variable than integrating for the curvilinear coordinate s. Similarly, the energy equation is rewritten

$$\frac{r_s^2 \sin\Gamma_s}{1-n\kappa_s}\frac{\partial H}{\partial r_s^2} - \left\{\frac{\eta \sin\Gamma_s}{1-n\kappa_s} + \frac{\cos\Gamma_s}{r_s}\left[\frac{\mu}{RePr} + \frac{2}{Re}\frac{r^2}{r_s^2}\frac{\partial}{\partial\eta}\left(\frac{\rho\mu F}{Pr}\right)\right]\right\} \times \frac{\partial H}{\partial\eta} - \frac{2}{Re}\frac{\cos\Gamma_s}{r_s}\left(\frac{r}{r_s}\right)^2 \frac{\rho\mu F}{Pr}\frac{\partial^2 H}{\partial\eta^2} = \frac{\cos^3\Gamma_s}{r_s Re}\left[\frac{2M_\infty^2(\gamma_\infty - 1)}{2 + M_\infty^2(\gamma_\infty - 1)}\right] \times \left\{\left[\left(\mu - \frac{\mu}{Pr}\right) + \left(\frac{r^2}{r_s^2}\right)\frac{\partial}{\partial\eta}\left(\rho\mu F - \frac{\rho\mu F}{Pr}\right)\right]\frac{\partial F^2}{\partial\eta} + \rho F\left(\frac{r^2}{r_s^2}\right)\left(\mu - \frac{\mu}{Pr}\right)\frac{\partial^2 F^2}{\partial\eta^2}\right\} \tag{22}$$

By integrating Eq. (7), the coordinate normal to the shock can be obtained from

$$n - n^2\frac{\cos\Gamma_s}{2r_s} = \frac{r_s}{2}\int_\eta^1 \frac{d\eta}{\rho F} \tag{23}$$

Solving the quadratic for n,

$$n = \frac{r_s}{\cos\Gamma_s}\left[1 - \left(1 - \int_\eta^1 \frac{d\eta}{\rho F}\right)^{1/2}\right] \tag{24}$$

The last equation can be used to calculate the shock standoff distance by integrating across the shock layer to the body streamline $\eta = 0$.

In order to retain the parabolic nature of the equation set, a normal velocity distribution across the shock layer must be assumed. In a fashion similar to the approximation made by Maslen for the normal velocity gradient, Zoby and Graves[13] suggested that a first approximation can be obtained from

$$v(s,\eta) = v_s(s)\eta \tag{25}$$

Stagnation Line Solution

An important result of the governing equations in the above form is that by taking the limit as $s \to 0$, these equations may be solved as ordinary differential equations along the stagnation line. The limiting form of the streamwise momentum equation is

$$\kappa_s F^2 - \eta\kappa_s\frac{\partial F^2}{\partial\eta} - \mu\frac{\kappa_s^2}{Re}\frac{\partial F^2}{\partial\eta} - 2\frac{\kappa_s^2}{Re}\left[1 - \kappa_s n\right]^2 F\frac{\partial}{\partial\eta}\left[\rho\mu\frac{\partial F^2}{\partial\eta}\right] = \lim_{s\to 0}\left\{-\frac{1}{\rho u_s}\frac{\partial p}{\partial s}\bigg|_\eta\right\} + \lim_{s\to 0}\eta\left\{\frac{1}{\rho u_s}\frac{\partial^2 p}{\partial s\,\partial\eta} + \frac{1}{u_s}\frac{\partial p}{\partial\eta}\left(\frac{\partial}{\partial s}\frac{1}{\rho}\right) + \frac{1}{2u_s}\frac{\partial^2 v^2}{\partial s\,\partial\eta}\right\} \tag{26}$$

where for a perfect gas,

$$\lim_{s\to 0} -\frac{1}{u_s}\frac{\partial p}{\partial s}\bigg|_\eta = \left[\frac{\gamma+5}{\gamma+1} - \eta\right]\kappa_s + \left(\frac{\eta^2-1}{4}\right)\left[\frac{v_s}{\kappa_s^2}\frac{\partial\kappa_s}{\partial r_s^2} - 4\left(\frac{\gamma-1}{\gamma+1}\right)\right] \tag{27}$$

$$\lim_{s\to 0}\frac{1}{u_s}\frac{\partial^2 p}{\partial s\,\partial\eta} = \kappa_s - \left(\frac{\eta}{2}\right)\left[\frac{v_s}{\kappa_s^2}\frac{\partial\kappa_s}{\partial r_s^2} - 4\left(\frac{\gamma-1}{\gamma+1}\right)\right] \tag{28}$$

$$\lim_{s\to 0}\frac{1}{u_s}\frac{\partial^2 v^2}{\partial s\,\partial\eta} = \frac{4\eta\kappa_s}{\rho_{so}(\gamma+1)}\left[\frac{2}{M_\infty^2} - \left(\gamma - 1\right)\right] \tag{29}$$

Valid for inviscid flow, a first approximation to the streamwise derivative of the reciprocal of the density is obtained from

$$\lim_{s\to 0}\frac{1}{u_s}\frac{\partial}{\partial s}\left(\frac{1}{\rho}\right) = \frac{1}{\rho p}\left[-\frac{1}{u_s}\frac{\partial p}{\partial s}\right] - \left(\frac{\gamma-1}{2\gamma}\right)\left\{\frac{2\kappa_s}{p}\left[F^2 + \frac{\eta^2}{\rho_{so}}\left(\frac{4}{(\gamma+1)M_\infty^2} - \frac{1}{\rho_{so}}\right)\right]\right\} \tag{30}$$

An iterative process is used to update $(1/u_s)(\partial/\partial_s)(1/\rho)$ so that the derivative is consistent with the viscous solution. The above equation is used to start the solution along the stagnation line. The procedure then marches downstream one station, calculates a viscous value for $(1/u_s)(\partial/\partial_s)(1/\rho)$, and returns to the stagnation line. This is repeated until the term converges. Equation (14) reduces to

$$p\left(0,\eta\right) = p_{so} - \frac{1}{2}\frac{\eta^2 - 1}{\rho_{so}} \tag{31}$$

and finally, the energy equation reduced very simply to

$$\left\{\eta + \frac{\kappa_s}{Re}\left[\frac{\mu}{Pr} + 2\left(1 - n\kappa_s\right)^2\frac{\partial}{\partial\eta}\left(\frac{\rho\mu F}{Pr}\right)\right]\right\}\frac{\partial H}{\partial\eta} + \frac{2\kappa_s}{Re}\left[1 - n\kappa_s\right]^2\frac{\rho\mu F}{Pr}\frac{\partial^2 H}{\partial\eta^2} = 0 \tag{32}$$

Solving the Governing Equations

The solution of the governing equations is relatively straightforward since the shock shape is assumed and then updated iteratively. A fully implicit method is used to solve the streamwise momentum [Eq. (20)] and energy [Eq. (22)] equation for the tangential velocity component and the total enthalpy along a line normal to the shock. The normal momentum equation is replaced by Maslen's second-order approximate integral [Eq. (14)] and the assumed normal velocity component distribution [Eq. (27)]. The streamwise momentum equation is linearized using the quasilinearization process suggested by Blottner,[18] where for example,

$$F = \frac{F^2 + \bar{F}^2}{2\bar{F}} \tag{33}$$

$$F\frac{\partial^2 F^2}{\partial\eta^2} = F\frac{\partial^2\bar{F}^2}{\partial\eta^2} + \bar{F}\frac{\partial^2 F^2}{\partial\eta^2} - \bar{F}\frac{\partial^2 2\bar{F}^2}{\partial\eta^2} = \frac{F^2}{2\bar{F}}\frac{\partial^2\bar{F}^2}{\partial\eta^2} + \bar{F}\frac{\partial^2 F^2}{\partial\eta^2} - \frac{\bar{F}}{2}\frac{\partial^2\bar{F}^2}{\partial\eta^2} \tag{34}$$

Convergence of the quasilinearization technique usually is obtained in three to five iterations. Second-order central and backward differences are used in the η and r_s^2 directions, respectively, so that the streamwise momentum and energy equations can be written

$$\alpha_1\frac{\partial F^2}{\partial r_s^2} + \alpha_2\frac{\partial F^2}{\partial\eta} + \alpha_3\frac{\partial^2 F^2}{\partial\eta^2} + \alpha_4 F^2 = \alpha_5 \tag{35}$$

$$\alpha_6\frac{\partial H}{\partial r_s^2} + \alpha_7\frac{\partial H}{\partial\eta} + \alpha_8\frac{\partial^2 H}{\partial\eta^2} = \alpha_9 \tag{36}$$

The Thomas algorithm[19] is then used to solve the resulting tridiagonal matrices to determine the tangential velocities and then the total enthalpy in successive iterations along a line normal to the shock. Once the tangential velocities and total

enthalpies are obtained, the shock standoff distance is determined from Eq. (24). This standoff distance is then compared with the extrapolated geometric distance between the shock and the body. The error between the two distances is then used in updating the shock shape as described in the next section.

The grid used by Ref. 4 is employed and consists of three regions. Points are clustered with a geometric progression near the wall, with a linear distribution near the shock, and an exponential fit between the two distributions. Typically, 41 to 101 points are required across the shock layer to resolve the viscous effects. The stepsize in the s direction is halved or doubled as necessary to hold the number of iterations required to obtain a converged shock shape between five and fifteen.

The approximate method may also be used to calculate transitional and turbulent flows and flows with air in chemical equilibrium as with the VSL method. The Cebeci-Smith[20] model, a two-layer algebraic eddy viscosity method that approximates the effects of the pressure gradient in the inner layer, is used for turbulent modeling. The outer layer model is that given by Clauser[21] and Klebanoff.[22] During transition to turbulence, the composite eddy viscosity is modified using the Dhawan and Narashima[23] method. Thermodynamic and transport properties for equilibrium air calculations are obtained from the tables of Hansen.[24]

Solving the Direct Problem

Since the method of Maslen is inverse in nature, an iterative procedure is necessary in order to obtain the correct shock shape for the prescribed body. In the stagnation and nose region where the flow is transonic, the shock shape must be determined in a global fashion. For smooth, convex nose shapes, the shock standoff distance varies slowly with the distance along the shock. Approximating the derivative of n_b in terms of the body radius results in the equation

$$\frac{dn_b}{ds} = \sin\left(\Gamma_s - \Gamma_b\right) \cong \alpha r_b + \beta r_b^3 \tag{37}$$

which can be integrated directly for the standoff distance

$$n_b = n_{bo} + \alpha \int_0^s r_b ds_b + \beta \int_0^s r_b^3 \, ds_b \tag{38}$$

where

$$n_{bo} = \left(n_b \kappa_s\right)_o \frac{1}{[1 - (n_b \kappa_s)_o][\kappa_{bo} - \alpha]} \tag{39}$$

During a given iteration, a shock shape is described by specifying α and β. The governing equations are solved along the stagnation line and then marched downstream around the body nose to the end of the subsonic nose region as in many boundary-layer techniques. The correct standoff distance at the stagnation point is already incorporated as part of the shock shape description. At two other points along the shock surrounding the nose region, the standoff distance obtained from the integration of Eq. (24) is compared to the geometric distance between the curve describing the shock and the curve describing the body. The error in the shock standoff distance at these two points is then used to update α and β using a Newton-Raphson iterative technique. The process is repeated until the shock shape converges, typically within 10–20 iterations. If the nose region is described using a conic section, the integrals of [Eq. (40)] may be evaluated analytically. The shock curvature and its derivative along the shock are also required and are calculated as follows:

$$\kappa_s = \frac{g_1}{g_2} \tag{40}$$

$$\frac{d\kappa_s}{ds} = \left(\frac{1}{g_2^2}\right)\left\{\cos\left(\Gamma_s - \Gamma_b\right)\frac{\partial g_1}{\partial s} + g_1 \sin\left(\Gamma_s - \Gamma_b\right)\left[\kappa_b \frac{\partial s_b}{\partial s_s} - \kappa_s\right] - g_1^2 \frac{\partial n_b}{\partial s_b}\frac{\partial s_b}{\partial s_s}\right\}$$

where

$$g_1 = \kappa_b - \frac{(\alpha + 3r_b^2\beta)\sin\Gamma_b}{\cos(\Gamma_s - \Gamma_b)} \tag{41}$$

$$g_2 = \cos(\Gamma_s - \Gamma_b) + n_b g_1 \tag{42}$$

$$\frac{\partial s_b}{\partial s_s} = \frac{1 - n_b \kappa_s}{\cos(\Gamma_s - \Gamma_b)} \tag{43}$$

and

$$\frac{\partial g_1}{\partial s} = \frac{\partial \kappa_b}{\partial s_b}\frac{\partial s_b}{\partial s_s} + \frac{1}{\cos^2(\Gamma_s - \Gamma_b)} \times \left\{\left(\alpha + 3\beta r_b^2\right)\sin\Gamma_b \sin\left(\Gamma_s - \Gamma_b\right)\left[\kappa_b \frac{\partial s_b}{\partial s_s} - \kappa_s\right]\right\} - \frac{\partial s_b}{\partial s_s}\frac{[\sin^2\Gamma_b(6\beta r_b) + (\alpha + 3\beta r_b^2)\kappa_b \cos\Gamma_b]}{\cos(\Gamma_s - \Gamma_b)} \tag{44}$$

A marching technique may be used once the flow transitions from the transonic nose region to the supersonic inviscid flow of the afterbody region. The solution for the nose region is ended when the local Mach number just inside the shock exceeds 1.80. This empirically determined criteria assures that the points along a line normal to the shock and extending into the body are supersonic except for a few points deep in the boundary layer. The shock shape (position, slope, and curvature) are determined as the solution is marched along the body. The shock is extrapolated from x_{s1} to x_{s2}

$$r_{s2} - r_{s1} = A(x_{s2} - x_{s1}) + B(x_{s2} - s_{s1})^2 + C(x_{s2} - x_{s1})^3 \tag{45}$$

where the shock slope and radius of curvature at the previous station ($s1$) constrain the constants A and B. The shock angles and curvature are calculated using the following relations:

$$\Gamma_s = \tan^{-1}\frac{\partial r_s}{\partial x_s} \tag{46}$$

$$\kappa_s = -\cos^3\Gamma_s \frac{\partial^2 r_s}{\partial x_s^2} \tag{47}$$

$$\frac{\partial \kappa_s}{\partial s} = \cos^4\Gamma_s\left\{-\frac{\partial^3 r_s}{\partial x_s^3} + \frac{3\kappa_s^2 \sin\Gamma_s}{\cos^4\Gamma_s}\right\} \tag{48}$$

The constant C is updated iteratively using a Newton-Raphson technique by comparing the shock standoff distance obtained from the flowfield solution to the distance between the shock and body determined from the geometry of the extrapolated shock. Once the standoff distances agree to within the desired tolerance, the solution is marched downstream to the next x station and the process repeated.

Results

In order to cover the capabilities and limitations of the present engineering method within the limited space of this paper, representative comparisons with the more detailed viscous shock-layer solutions of Ref. 25 and experimental data are presented. Beginning with a brief look at the computational effort typically required, results are then given for the surface heat transfer and pressure distribution for laminar, transitional, and turbulent flow over sphere cones at zero angle of attack. Selected shock-layer profile comparisons are also presented. Finally, the ability to provide viscous starting shock shapes to the VSL method is addressed.

Table 1 Comparison of execution times for the approximate and full viscous shock-layer equations

Method	Grid	Iteration	Time, CPU, s
(a) 30-deg sphere cone, CYBER 180-360			
NSWC	—	Inviscid shock shape	28.6
VSL	177×101×1	1st Global	80.41
		2nd Global	79.22
		Total	188.23
Present	153×101×1	Total	88.54
(b) 15-deg sphere cone, SUN3/280			
NSWC	—	Inviscid shock shape	—
VSL	216×101×1	1st Global	404.7
		2nd Global	407.1
		Total	811.8
Present	120×101×1	Total	372.7
VSL	216×61×1	1st Global	256.3
		2nd Global	253.0
		Total	509.3
Present	120×61×1	Total	261.1

Table 2 Comparison of stagnation heat-transfer rates for the approximate and full viscous shock-layer equations

Re_{R_n}	Grid	VSL,[25] $\dot{q}_{wo}$, Btu/ft²s	Present method, $\dot{q}_{wo}$, Btu/ft²s	% Diff.
(a) 15-deg sphere cone, Cleary[27]				
37,500	101	−34.83	−34.61	1.77
	61	−33.26	−33.43	0.63
110,000	101	−19.72	−20.07	0.51
(b) 5-deg sphere cone, $\alpha = 0$ deg[25]				
19,033	101	−404.8	−400.5	1.07
114,200	101	−163.9	−161.8	1.29

Table 1 documents several timings made between the present and VSL methods. The first case is a 30-deg sphere cone run on a Control Data CYBER 180-860. The freestream conditions were $M_\infty = 10$ and $Re = 7000$ and the calculations were ended at $s_b/R_n = 40.0$. The grids were both fixed at 101 points in the n direction, but varied in the s direction with 153 points for the present method and 177 points for the VSL method. The VSL method requires a starting shock shape which is obtained from the NSWC inviscid method.[26] It is apparent that the computational time required to make one global iteration with the VSL equations and a complete solution with the approximate equations are equivalent, 80.4 s vs 88.5 s. However, the VSL method requires a starting solution and typically two global iterations to obtain residual errors in the shock standoff distance of less than 1-3%. The approximate method develops the shock shape as the calculations proceed around the body with residual errors in the shock standoff distance of 1% in the nose region and less than one-hundredth of a percent in the afterbody region. Although the convergence criteria is very tight in the afterbody region, it is necessary for smooth shock shapes in the vicinity of the surface pressure minimum and as the solution approaches sharp cone results. Summing the execution times for the starting solution and two global iterations of the VSL method and dividing by the number of grid points yields an execution speed of 94.7 points/s. The approximate method performs at 174.53 grid points/s or 1.84 times faster. The second and third cases are for the $M_\infty = 10.6$, $Re = 37{,}500$ flow over a 15-deg sphere cone from the experiments of Cleary.[27] The computations were halted at $s_b/R_n = 50.0$. Coarse and fine grids were run using the two methods on a SUN 3/280 computer. The NSWC starting shock shape was obtained on a CYBER machine and so execution times were not comparable. The trends noted above are again evident. The present method performs at 32.52 and 28.04 grid points/s for the 101 and 61 point grids, respectively. The corresponding speeds for the VSL method neglecting the starting solution (which accounted for 15% of the execution time in the first case) are 26.87 and 25.87 points/s. It is important to note that these calculations were performed on scalar machines. Although moderate reductions in execution time could be realized through vectorization for the present method, significant reductions could be obtained using parallel computer architectures.

The laminar heat-transfer data of Cleary[27] for a 15-deg sphere cone in a perfect gas flow at Mach 10.6 is compared in Fig. 2 with both the present method and with VSL. The agreement between the present method, VSL, and the experimental data is very good. The stagnation-point heating rates are within 2% of the VSL calculations, as indicated in Table 2. An experimental value is not available for comparison. Additionally, the approximate method is slightly conservative in comparison to the VSL method in predicting the surface heat transfer on the conical afterbody. Although not shown, the surface pressure predictions from the present method agreed very well with VSL and experimental data.

Several typical shock-layer profiles for the $Re = 110{,}000$ case are given in Figs. 3-5. The data are plotted for two axial stations: $x/R_n = 0$, the stagnation line, and $x/R_n = 12.53$, midway through the pressure recompression on the cone. The ordinate for the figures corresponds to the distance normal to the wall. At the stagnation point, and the aft station, shock standoff distances differed by less than 1 and 5%, respectively. All of the profiles compare very well between the two theories. In particular, note the excellent agreement between pressure distributions. The discrepancy in the pressure at the shock at the aft station reflects the slightly different shock shapes predicted by the two methods in the pressure recovery region. In Fig. 4, the assumed normal velocity component distribution is compared with the calculated values. Along the stagnation line, the comparison is excellent, while at the downstream station the profiles differ near the wall. Note, however, at the aft station and further downstream, that the normal velocity component is very small in comparison to the tangential component. As would be expected, the comparison between shock shapes and shock-layer profiles improves to excellent downstream as the recompression to sharp cone results proceeds. Density and temperature profiles across the shock layer also compare very well between the two methods, although they are not presented here.

In Figs. 6 and 7, the present method and VSL calculations[25] are compared for the Mach-15 perfect-gas flow over a very

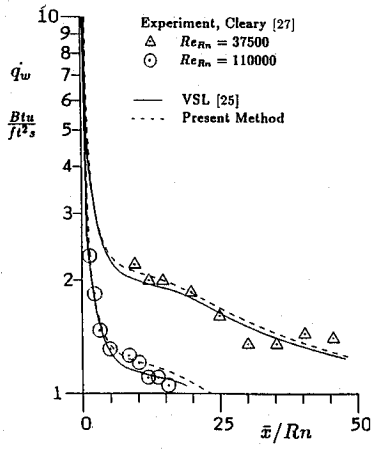

Fig. 2 Laminar heat-transfer rate distributions for a 15-deg sphere cone ($M_\infty = 10.6$, $T_o = 2000°$R, $T_w = 540°$R).

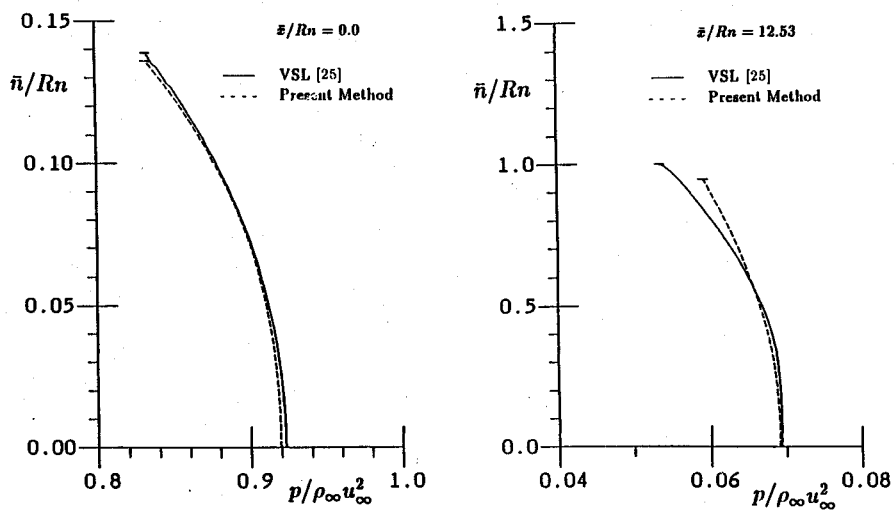

Fig. 3 Distribution of pressure across the shock layer of a 15-deg sphere cone ($M_\infty = 10.6$, $Re_{R_n} = 110{,}000$, $T_o = 2000°R$, $T_w = 540°R$).

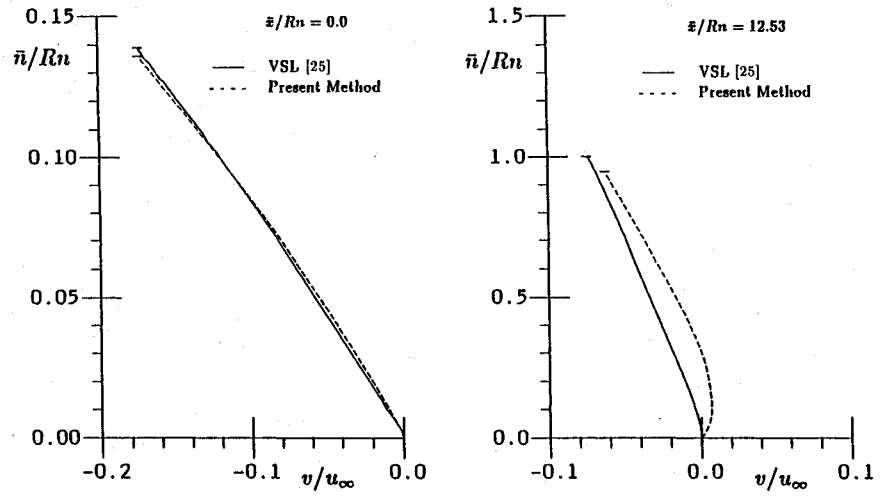

Fig. 4 Distribution of tangential velocity component across the shock layer of a 15-deg sphere cone ($M_\infty = 10.6$, $Re_{R_n} = 110{,}000$, $T_o = 2000°R$, $T_w = 540°R$).

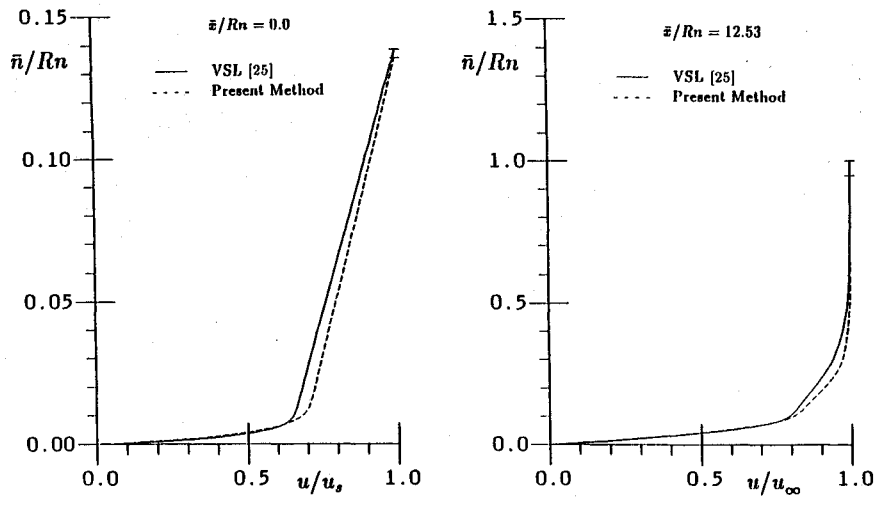

Fig. 5 Distribution of normal velocity component across the shock layer of a 15-deg sphere cone ($M_\infty = 10.6$, $Re_{R_n} = 110{,}000$, $T_o = 2000°R$, $T_w = 540°R$).

long 5-deg sphere cone. The transition points were calculated empirically[25] and were identical for both methods. The laminar, transitional, and turbulent heating rates show good agreement in Fig. 6. The stagnation-point heat-transfer rates compare very well between the two methods as indicated in Table 2. Figure 7 shows that the surface pressures predicted by the present method agree well with VSL calculations. The increased surface pressure after transition indicates that the methods have adjusted their respective shock shapes to accommodate the increased displacement thickness of the turbulent

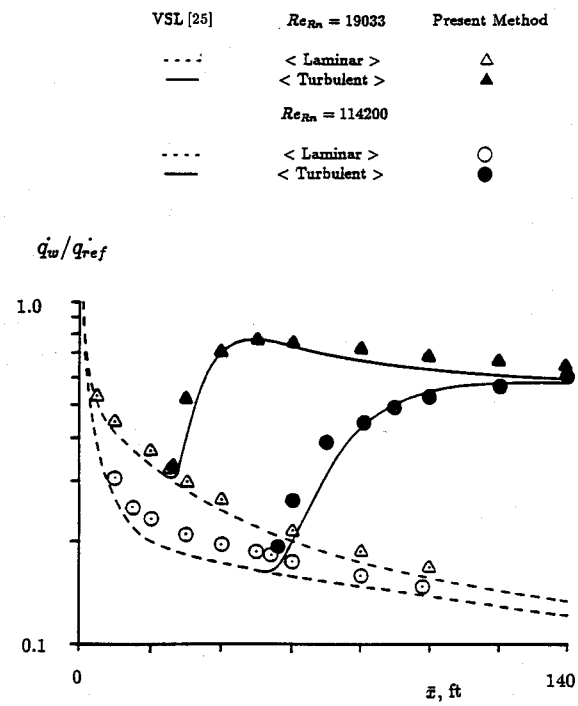

Fig. 6 Surface heat-transfer rate distributions for the perfect gas flow over a 5-deg sphere cone ($M_\infty = 15$, $h = 150$ Kft, $T_\infty = 480°R$, $T_w = 2260°R$).

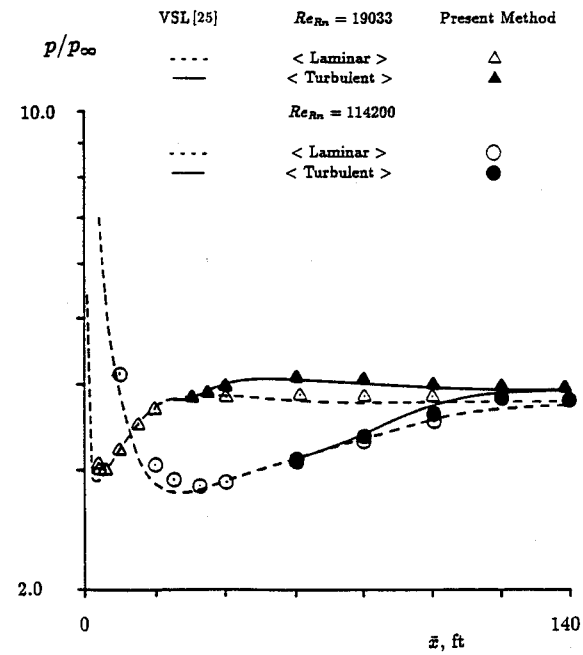

Fig. 7 Surface pressure distributions for the perfect gas flow over a 5-deg sphere cone ($M_\infty = 15$, $h = 150$ Kft, $T_\infty = 480°R$, $T_w = 2260°R$).

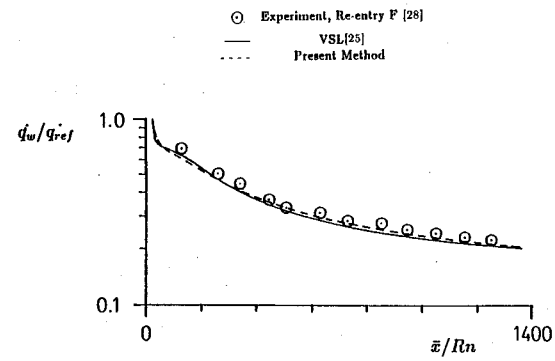

Fig. 8 Surface heat-transfer rate distributions for the equilibrium airflow over a 5-deg sphere cone ($M_\infty = 19.25$, $h = 120$ Kft, $Re_{R_n} = 7519$, $R_n = 0.114$ in.).

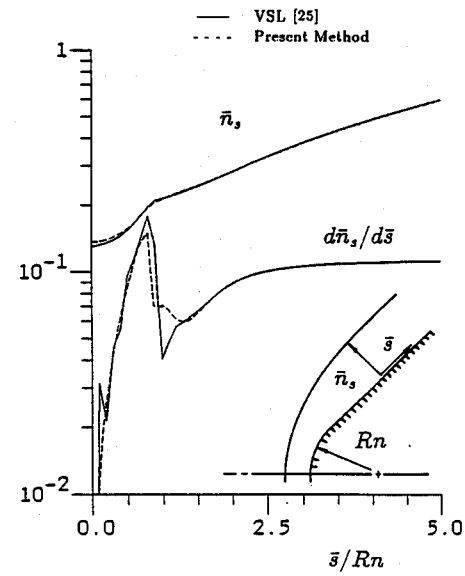

Fig. 9 Distribution of shock standoff distance and its derivative with respect to body surface arc length for a 45-deg sphere cone ($M_\infty = 10.6$, $Re_{R_n} = 1.0 \times 10^6$, $T_\infty = 480°R$, $T_w = 2260°R$).

boundary layer. Such a result would be missed by a noniterative inviscid/boundary-layer method.

An experiment known as Re-entry F[28] was performed in 1968 to provide laminar, transitional, and turbulent heating data on a slender conical body during free flight at Mach numbers near 20. The Re-entry F vehicle was a 5-deg sphere cone, 13 ft in length with an initial nose radius of 0.1 in. In Fig. 8, laminar heat-transfer predictions for the present method and VSL are compared with the flight test data of 120,000 ft. Both codes assume that the $M_\infty = 20$ flow is in chemical equilibrium. Agreement between the two methods and the flight test data is excellent.

For many low Reynolds number flows, using an inviscid starting solution for a VSL method implies that many global iterations will be needed to properly converge the viscous shock shape. In other instances, starting shock shapes are difficult to obtain for large-angle sphere cones. The NSWC code, for example, is limited to sphere cones with half-angles of less than 30 deg because the axial component of Mach number on the conical afterbody must exceed one. For either of these situations, the present method could be used to provide an accurate viscous shock shape for a starting solution. In Fig. 9, the shock shape of the present method was used as a starting shock shape for the VSL method in calculating the flow over a 45-deg sphere cone. Distributions are presented of the body normal shock standoff distance and its derivative with respect to the body surface arc length. These distributions

define the starting shock shape obtained using the present method and the shock shape calculated by the VSL method after one global iteration. Note that the derivative dn_s/ds_b is accurately predicted by the approximate method.

Conclusions

An approximate method has been developed that can accurately calculate the surface and flowfield properties for the fully viscous flow over blunt-nosed axisymmetric bodies at zero angle of attack. The method is applicable to a wide range of freestream Mach and Reynolds numbers. However, the approximations incorporated into the method represent the full equations for Mach numbers of 10 and above. In addition, high Reynolds number flow with a very thin viscous layer in comparison to the inviscid layer could be calculated more economically using a coupled inviscid/boundary-layer method.

Numerous comparisons, some presented in this paper, have shown that the second-order approximate integral to the normal momentum equation developed by Maslen is accurate throughout the majority of the shock layer. Unpublished work of Riley and DeJarnette indicate that the error noted in the vicinity of the pressure minimum can be reduced by employing a better approximation to the normal velocity distribution.

Execution time comparisons have shown that the approximate method is faster than the full VSL method primarily because starting solutions and multiple global iterations are not required. The present method would be well suited to parallel architectures, further reducing run times. The actual clock time required to obtain a solution from the user's point of view is considerably reduced since intermediate smoothing and manipulation of the shock shapes is not required.

Finally, the results obtained using the approximate viscous shock-layer method have been very encouraging. Research is currently under way to extend this method to three-dimensional configurations and flowfields.

Acknowledgments

This research was supported by Cooperative Agreement NCC1-100 between North Carolina State University and the Aerothermodynamics Branch of the NASA Langley Research Center. Many thanks are due to E. Vincent Zoby, the technical officer, and to the other members of the Aerothermodynamics Branch who graciously contributed their time and expertise.

References

[1]Hekkiwell, W. S., Dickson, R. P., and Lubard, S. C., "Viscous Flow over Arbitrary Geometries at High Angles of Attack," *AIAA Journal*, Vol. 19, No. 2, 1981, pp. 191–197.

[2]Gnoffo, P. A., "Hypersonic Flows over Biconics Using a Variable-Effect-Gamma, Parabolized Navier-Stokes Code," AIAA Paper 83-1666, July 1983.

[3]Davis, R. T., "Numerical Solution of the Hypersonic Viscous Shock-Layer Equations," *AIAA Journal*, Vol. 8, No. 12, 1970, pp. 2152–2156.

[4]Murray, A. L., and Lewis, C. H., "Hypersonic Three-Dimensional Viscous Shock-Layer Flows over Blunt Bodies," *AIAA Journal*, Vol. 16, No. 12, 1978, pp. 1279–1286.

[5]McWherter, O. M., Noack, R. W., and Oberkampf, W. L., "Evaluation of Inviscid/Boundary-Layer and Parabolized Navier-Stokes Solutions for Design of Re-entry Vehicles," AIAA Paper 84-0486, Jan. 1984.

[6]DeJarnette, F. R., and Hamilton, H. H., "Inviscid Surface Streamlines and Heat Transfer on Shuttle-Type Configurations," *Journal of Spacecraft and Rockets*, Vol. 10, No. 3, 1973, pp. 314–321.

[7]Anderson, E. C., Moss, J. N., and Sutton, K., "Turbulent Viscous Shock-Layer Solutions with Strong Vorticity Interaction," *Journal of Spacecraft and Rockets,* Vol. 14, No. 3, 1977, pp. 257-264.

[8]Goodrich, W. D., Li, C. P., Houston, C. K., Chiu, P. B., and Olmedo, L., "Numerical Computations of Orbiter Flowfields and Laminar Heating Rates," *Journal of Spacecraft and Rockets,* Vol. 14, No. 3, 1977, pp. 257–264.

[9]Hamilton, H. H., DeJarnette, F. R., and Weilmuenster, K. J., "Application of Axisymmetric Analogue for Calculating Heating in Three-Dimensional Flows," *Journal of Spacecraft and Rockets*, Vol. 24, No. 4, 1987, pp. 296–302.

[10]Zoby, E. V., and Simmonds, A. L., "Engineering Flowfield Method with Angle-of-Attack Applications," *Journal of Spacecraft and Rockets,* Vol. 22, No. 4, 1985, pp. 398–404.

[11]Maslen, S. H., "Inviscid Hypersonic Flow Past Smooth Symmetric Bodies," *AIAA Journal,* Vol. 5, No. 6, 1964, pp. 1055–1061.

[12]Maslen, S. H., "Asymmetric Hypersonic Flow," NASA CR-2133, Sept. 1971.

[13]Zoby, E. V., and Graves, R. A., Jr., "A Computer Program for Calculating the Perfect Gas Inviscid Flowfield About Blunt Axisymmetric Bodies at an Angle of Attack of 0 Deg," NASA TM-X2843, Dec. 1973.

[14]Grose, W. L., "An Approximate Solution to the Nonequilibrium Flow in the Inviscid Shock Layer About a Vehicle in Hypersonic Flight in an Arbitrary Atmosphere," Ph.D. Diss., Virginia Polytechnic Inst., Blacksburg, VA, June 1969.

[15]Davis, R. T., "A Procedure for Solving the Compressible Interacting Boundary-Layer Equations for Subsonic and Supersonic Flows," AIAA Paper 84-1614, June 1984.

[16]Anderson, E. C., and Moss, J. N., "Numerical Solution of the Hypersonic Viscous Shock-Layer Equations for Laminar, Transitional, and Turbulent Flows of a Perfect Gas over Blunt Axially Symmetric Bodies," NASA TN-D-7865, Feb. 1975.

[17]Thareja, R. R., Szema, K. Y., and Lewis, C. H., "Chemical Equilibrium Laminar or Turbulent Three-Dimensional Viscous Shock-Layer Flows," *Journal of Spacecraft and Rockets,* Vol. 20, No. 5, 1983, pp. 454–460.

[18]Blottner, F. G., "Introduction to Computational Techniques for Boundary Layers," Sandia Lab., Albuquerque, NM, SAND 79-0893, 1979.

[19]Anderson, D. A., Tannehill, J. C., and Pletcher, R. H., *Computational Fluid Mechanics and Heat Transfer*, Hemisphere, New York, 1984, pp. 128–129.

[20]Cebeci, T., "Behavior of Turbulent Flow near a Porous Wall with Pressure Gradient," *AIAA Journal*, Vol. 8, 1970, pp. 2152–2156.

[21]Clauser, F. H., "The Turbulent Boundary Layer," *Advances in Applied Mechanics,* Vol. IV, edited by H. L., Fryden and T. von Karmen, Academic, New York, 1956, pp. 1–51.

[22]Klebanoff, P. S., "Characteristics of Turbulence in a Boundary Layer with Zero Pressure Gradient," NASA Rept. 1247, 1955.

[23]Dhawan, S., and Narashima, R., "Some Properties of Boundary-Layer Flow During Transition from Laminar to Turbulent Motion," *Journal of Fluid Mechanics,* Vol. 3, Pt. 4, 1958, pp. 418–436.

[24]Hansen, C. F., "Approximations for the Thermodynamic and Transport Properties of High Temperature Air," NASA TR-R-50, 1959.

[25]Thompson, R. A., Zoby, E. V., Wurster, K. E., and Gnoffo, P. A., "An Aerothermodynamic Study of Slender Conical Vehicles," AIAA Paper 87-1475, June 1987.

[26]Solomon, J. M., Ciment, M., Ferguson, R. E., Bell, J. B., and Wardlaw, A. B., Jr., "A Program for Computing Steady Inviscid Three-Dimensional Supersonic Flow on Re-entry Vehicles, Vol. I, Analysis and Programming; Vol II, Users Manual," Rept. NSWC/WOL/TR 77-28, Feb. 1977.

[27]Cleary, J. W., "Effects of Angle of Attack and Bluntness on Laminar Heating-Rate Distributions on a 15-Deg Cone at a Mach Number of 10.6," NASA TN-5450, Oct. 1969.

[28]Stainback, P. C., Johnson, C. B., Boney, L. B. and Wicker, K. C., "Comparison of Theoretical Predictions and Heat-Transfer Measurements for a Flight Experiment at Mach 20 (Re-entry F)," NASA TM-X-2560, 1972.

Clark H. Lewis
Associate Editor